Diamond & Related Materials 97 (2019) 107426

Contents lists available at ScienceDirect

Diamond & Related Materials

journal homepage: www.elsevier.com/locate/diamond

Effect of ethanol soaking on the structure and physical properties of carbon nanocoils

Chenghao Deng[a,b], Peng Wang[b], Chengwei Li[b], Xinwei Wang[c], Lujun Pan[b,*]

[a] Center on Nanoenergy Research, School of Physical Science and Technology, Guangxi University, Naning 530004, PR China
[b] School of Physics, Dalian University of Technology, No. 2 Linggong Road, Ganjingzi District, Dalian 116024, PR China
[c] 2010 Black Engineering Building, Department of Mechanical Engineering, Iowa State University, Ames, IA 50011, United States of America

A B S T R A C T

Carbon nanocoils (CNCs), which are quasi-one-dimensional nanomaterials, exhibit a unique helical morphology and polycrystalline-amorphous structure. In this study, we investigated the effect of ethanol soaking on the structure and physical properties of CNCs. The CNCs were soaked in ethanol for up to one year. Structural examinations revealed that ethanol permeated into the CNCs through defects and vacancies. The permeation of ethanol molecules increased the stress inside the CNCs, resulting in the rearrangement of their sp^2 grains, which alleviated the stress. This improved the coherence of graphite grains. Meanwhile, the permeation of ethanol molecules separated the sp^2 grains and graphite layers within the grains. Prolonged soaking resulted in a gradual change in the chemical structure of the CNCs. After 346 days of soaking, the contents of both the C-O- and C = O bonds increased, resulting in a decrease in the C:O atomic ratio from 48 to 29. The increase in the C-O- and C = O bond contents facilitated the transformation of the sp^2 sites to other saturation sites. These physical and chemical changes in the structure of the CNCs reduced the concentration of conduction electrons and enhanced the electron hopping barrier and phonon scattering, thus reducing their electrical conductivity and thermal diffusivity significantly.

1. Introduction

The landmark discovery of carbon nanotubes (CNTs) by Ijima provided motivation for the development of one-dimensional (1D) nanomaterials [1]. The helical structure of CNTs was first theoretically predicted by Ihara and Dunlpan [2], and was then demonstrated using a transmission electron microscope (TEM) by Zhang et al. [3] Carbon nanocoils (CNCs) are helical CNTs with more or less defects [4–6]. Owing to their helical morphology, CNCs find potential applications in wearable devices [7,8], micro/nanoelectromechanical systems [9,10], nanosensors [11,12], field emitters [13,14], wave absorbers [15,16] and energy devices [17,18].

Chemical vapor deposition (CVD) is the most widely used synthesis method for CNCs [19–21]. CVD-synthesized CNCs are a hybrid of sp^2 nanograins and amorphous sp^3 networks, and exhibit a polycrystalline-amorphous structure. The geometry and structure of CNCs can be controlled by adjusting the growth conditions such as the catalyst and substrate type and synthesis temperature. In order to realize their practical applications, various approaches such as acidizing [22], annealing [23,24], functional materials coating [25–27], and doping [14,28] have been used to modify the surface or internal structure of CNCs.

Annealing treatments such as furnace heating, joule heating, and laser heating are carried out to modify the internal structure of CNCs. In carbon nanomaterials, annealing results in the reconstruction of carbon atoms toward higher graphitization degrees. The effects of annealing on the mechanical and electrical properties of CNCs have been investigated systematically. The crystallinity of CNCs improves with an increase in the annealing temperature from 1000 to 2600 °C. When annealed at 2600 °C, CNCs exhibit crystallinity comparable to that of graphite [24]. Apart from improving the crystallinity of CNCs, annealing also results in the formation of a large number of loops at the edges of their sp^2 grains [23]. High-temperature annealing significantly affects their internal structure, resulting in the transformation of their nanocrystalline structure into the highly graphitized structure of helical multi-walled CNTs. The order degree and size of sp^2 grains are all increased. After annealing, the electrical conductivity of CNCs increases, while the shear modulus decreases owing to the enhanced sliding of their graphite layers.

Besides controlling the internal structure of CNCs, surface modification is another approach to realize their practical applications, especially electrochemical applications [28]. The purpose of surface modification is to break the *C-C* bonds on the surface of CNCs and introduce other functional groups. The most widely used methods for the surface modification of CNCs include acid treatment [29], doping [14], and surface oxidizing [22]. These treatments break the C-C bonds and increase the number of defects in CNCs. In addition, surface treatment generates a large number of sites and functional groups, which facilitate

* Corresponding author.
E-mail address: lpan@dlut.edu.cn (L. Pan).

https://doi.org/10.1016/j.diamond.2019.05.012
Received 4 March 2019; Received in revised form 2 May 2019; Accepted 13 May 2019
Available online 14 May 2019
0925-9635/

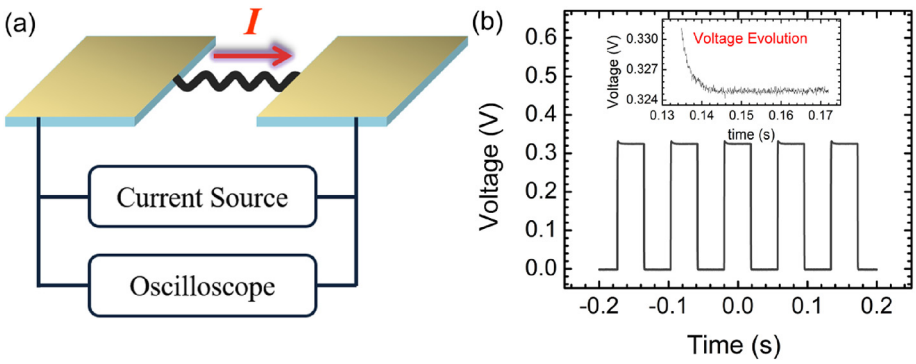

Fig. 1. (a) Schematic of the TET characterization of the suspended CNCs. (b) Typical voltage evolution signal of the CNCs. The inset shows the partially enlarged view.

the growth of other materials on the surface of CNCs.

Doping is an effective approach to modify the properties of CNCs. Chung et al. carried out high-temperature nitrogen post-doping of CNCs, which resulted in the formation of CN bonds in the CNCs and increased the number of sp^2 clusters. Nitrogen doping significantly improves the performance of CNC-based field emission lamps [14]. Jafri et al. used plasma nitrogen doping to modify CNCs, creating a large number of pyrrolic nitrogen defects on their surface [18]. These defects act as good anchoring sites for the deposition of Pt nanoparticles. Celorrio et al. carried out the liquid-phase treatment of CNCs using nitric acid, sulfuric acid, perhydrol, and their mixture [22]. All these liquids act as oxidants and introduce carboxylic and phenol groups on the surface of CNCs.

In this study, we developed a novel ethanol soak treatment method to modify both the internal structure and functional groups of CNCs. Ethanol, which is a common solvent, is a very weak liquid oxidant. Unlike acid or plasma treatments, the ethanol treatment was quite slow and induced both physical and chemical changes in the CNCs. We soaked the CNCs in ethanol for up to one year. The physical and chemical changes in the CNCs induced by ethanol soaking were examined. Various studies have been carried out to investigate the physical properties of CNCs. The relationship between the structure and physical properties of CNCs has also been investigated, for example, in the context of annealing. However, the relationship between the internal structure and physical properties of CNCs is still unclear. By examining the unique changes induced by ethanol soaking, we could analyze the effect of sp^2 grains and sp^3 networks on the thermal and electrical properties of CNCs, respectively.

2. Experimental

2.1. CVD synthesis and ethanol treatment of CNCs

The CNCs used in this study were synthesized using a CVD method [30]. First, a 0.2 mol/L solution consisting of $Fe_2(SO_4)_3{\cdot}9H_2O$, $SnCl_2{\cdot}5H_2O$, and deionized water, which acted as the catalyst precursor, was prepared. The catalyst was first dropped on the quartz substrate, which was then calcined at 710 °C for 30 min under the flow of Ar (365 sccm). At last, the carbon deposits were achieved at 710 °C for 1 h by introducing acetylene (flow rate = 15 sccm) and argon gases (flow rate = 325 sccm). After the CVD synthesis, the as-grown CNCs were dispersed in ethanol through ultrasonication and were then soaked in it for up to one year.

2.2. Structural characterization of CNCs

Raman spectroscopy and transmission electron microscopy (TEM) were used to examine the internal structures of the CNCs in order to analyze their structural changes induced by ethanol soaking. X-ray photoelectron spectroscopy (XPS) was employed to characterize the changes in the elemental composition and electronic structures of the CNCs. For Raman analysis, a suspension of the CNCs was dropped onto a glass substrate coated with a 36 nm-thick gold film, which acted as the enhancing substrate. Numerous CNC clusters were deposited on the substrate. These CNC clusters were irradiated with a 532-nm laser. The exposure time and stacking fold were 10 s and 4 times, respectively. Raman measurements were carried out in groups of five CNC clusters. The high-resolution TEM images and electron diffraction (ED) patterns of the CNCs were obtained using a TEM to analyze the changes in their size and the arrangement of sp^2 grains.

2.3. Electrical conductivity and thermal diffusivity of the ethanol-soaked CNCs

Changes in the structure of CNCs induce changes in their physical properties. The electrical conductivity of the CNCs was measured using a source meter (Agilent B2092A). The thermal diffusivity the CNCs was measured using the transient electro-thermal (TET) technique. The TET method, which was developed by Wang et al., is a simple and effective method for the thermal characterization of 1D or quasi-1D micro/nanomaterials [31] This method works on the principle of the temperature evolution (expressed as the resistance evolution when the resistance of the CNCs changes with temperature) of CNCs under joule heating in vacuum. A step current was applied to the CNCs and their resistance evolution was recorded using an oscilloscope. The thermal diffusivity of the CNCs could be calculated from their evolution curve. The schematic of the TET process and the typical voltage evolution curve of the CNCs are shown in Fig. 1. The inset in Fig. 1b shows a partially enlarged view. The thermal characterization procedures used in this study have been discussed in detail in our previous work [32].

3. Results and discussion

Fig. 2 shows the TEM images and ED patterns of the CNCs soaked in ethanol for different durations. Like multi-walled CNTs, the CNCs showed a hollow interior. The fiber diameter of the four CNCs shown in Fig. 2 was around 300 nm. The CNCs exhibited a unique polycrystalline-amorphous structure with nano sp^2 grains embedded in amorphous sp^3 networks. The ratio of sp^2 to sp^3 structures has been measured to be 4:1 through electron energy loss spectrum (EELS) by Chen et al. [33] X-Ray diffraction (XRD) studies have revealed that the average sp^2 grain size of CNCs is around 3.5 nm [32]. The sp^2 grains of CNCs are not uniformly aligned. As a whole, the internal structure of CNCs is almost amorphous. With an increase in the soak time from 0 to 180 days, the sp^2 grains showed slightly improved orientation coherence, as observed from Fig. 2c. The ED patterns of the CNCs confirmed the improvement in the sp^2 grain orientation. The ED patterns of the CNCs were circular, indicating that they were almost amorphous. The innermost circle

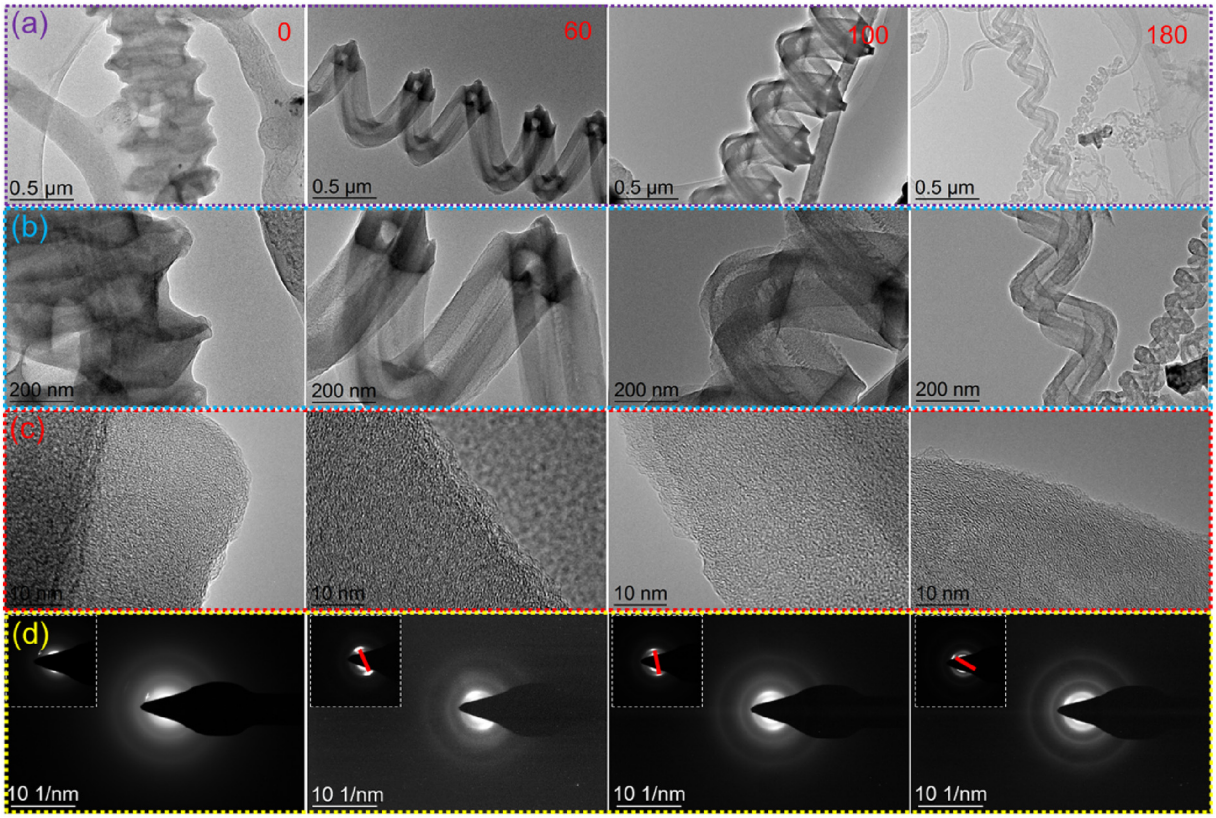

Fig. 2. (a) and (b) TEM images, (b) high-resolution TEM images and (c) ED patterns for the CNCs soaked for different durations (0–180 days). The insets in (d) are the ED patterns after brightness and contrast adjustment showing the changes in the (002) planes.

corresponds to the (002) plane of graphite. With an increase in the soak time, the ED patterns became finer, indicating the improvement in their crystallization consistency. We adjusted the brightness and contrast of the ED patterns through image processing software, as shown in the inset. With an increase in the soak time, the ED patterns of the (002) lattice plane transformed gradually from blurry circles to small arc-shaped patterns and the orientation of the sp^2 grains became more uniform.

From the ED patterns, we measured the interlayer spacing for the (002) plane of the CNC groups with three samples each. The (002) plane interlayer spacing increased (from 0.346 to 0.364 nm, increased by 5.2%) with an increase in the soak time, as shown in Fig. 3. Almost amorphous CNCs consist of a large number of defects, which facilitate the permeation of ethanol into them. Ethanol molecules distend the

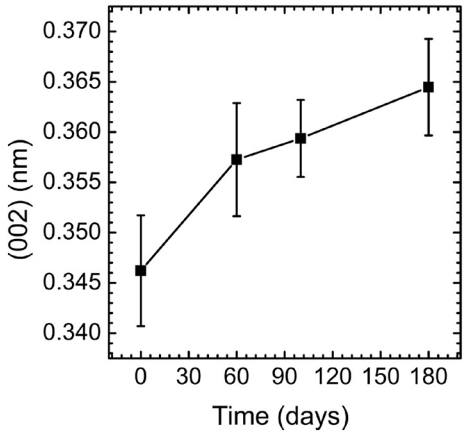

Fig. 3. Interlayer spacing of the (002) lattice plane for the CNCs soaked in ethanol for different durations.

graphite layers of CNCs, resulting in an increase in the (002) interlayer spacing. The interlayer spacing for all sp^2 grains becomes uniform with ethanol permeation, resulting in finer ED patterns. When ethanol fills the space between the graphite layers and the vacancies, an internal stress is generated. The sp^2 grains rearrange under this internal stress, resulting in the formation of ordered structures with reduced stress. This transformation improves the grain orientation.

Fig. 4 shows the XPS results of CNCs soaked in ethanol for 0 and 346 days. Using peak-fit processing, the characteristic spectra line for carbon (C) could be divided into four peaks, as shown in Fig. 4a and c. The two peaks around 284 eV correspond to sp^2 and sp^3 carbons, while the other two peaks correspond to CO- and COO- bonds. The characteristic spectra line for oxygen (O) could be divided into three peaks corresponding to the metal oxide and C=O and CO- bonds. These functional groups are similar to those of oxidized graphene [34]. The graphite layer plane consisted of C-O-, C-O-C, and C-OH bonds. COOH, COO-, and C=O bonds were observed at edge of the graphite layer. The metal oxide peak can be attributed to the catalyst particles. With an increase in the soak time, the metal oxide content decreased gradually. The sample soaked for 346 days showed no metal oxide peak, as shown in Fig. 4d. Ethanol soaking resulted in the removal of the catalyst particles from the CNCs. With an increase in the soak time from 0 to 346 days, the CO- and C=O bond contents increased by 90 and 125%, respectively, as calculated using the peak height of sp^2 carbons as the reference.

The C:O atomic ratio of the CNCs was calculated using the ratio of the area of the C and O bonds, as shown in Fig. 5. With an increase in the soak time from 0 to 346 days, the C:O atomic ratio decreased from 48 to 29 (by 39%).

With an increase in the soak time, ethanol gradually permeated into the CNCs, resulting in an increase in their oxygen content. Along with this physical permeation, some chemical reactions also proceeded slowly. Ethanol molecules decomposed into hydrogen and alkoxyl

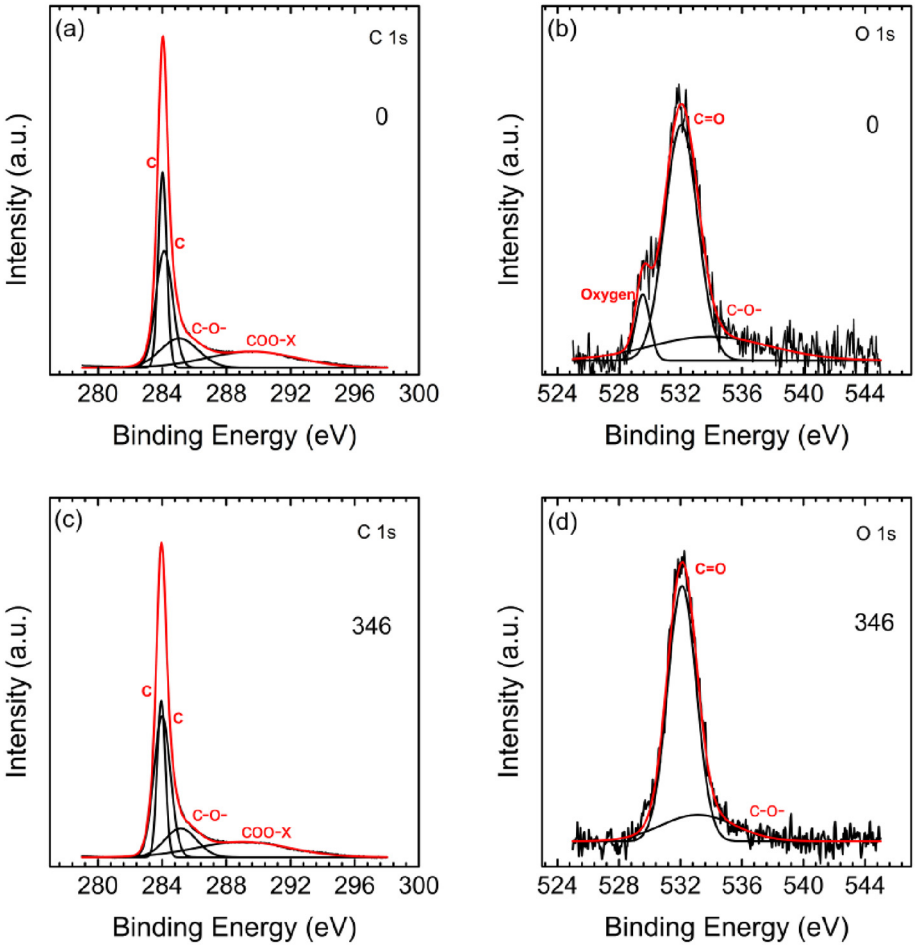

Fig. 4. XPS profiles of the CNCs soaked for 0 [(a) and (b)] and 346 [(c) and (d)] days.

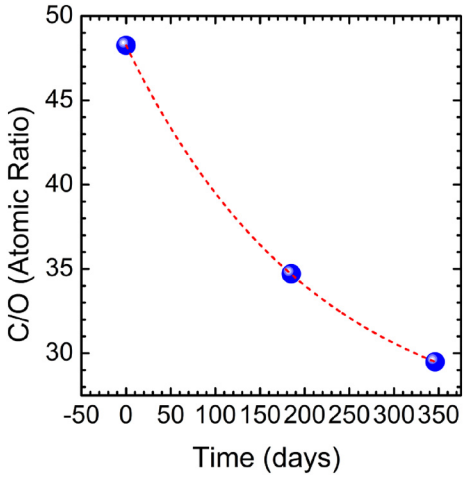

Fig. 5. C:O atomic ratio of the CNCs, as measured from the XPS results.

radicals. These radicals combined with the unoccupied states of carbon (*sp* and sp^2 carbon atoms), forming saturation states.

Raman spectroscopy was used to further examine the structural changes occurring in the CNCs (Fig. 6a). Graphite-like materials show two characteristic Raman peaks: D and G peaks [35]. The G peak corresponds to the in-plane bond-stretching motion of sp^2 carbon atom pairs. This mode does not require the presence of six-fold rings. It occurs at all sp^2 sites (not only in the rings). The D peak corresponds to the breath mode of six-fold rings. It is forbidden in pristine graphite and becomes active only in the presence of disorders. The intensity ratio of D to G peaks (I_D/I_G) is inversely proportional to the in-plane correlation length or cluster diameter.

Fig. 6b shows the I_D/I_G ratio of the CNCs as a function of the soak time. With an increase in the soak time from 0 to 120 days (stage 1) the I_D/I_G ratio decreased from 1.16 to 0.86. With an increase in the soak time from 120 to 180 days (stage 2) the I_D/I_G ratio increased from 0.86 to 1.20. In stage 1, the internal stress induced by ethanol permeation and the improvement in the sp^2 grain orientation suppressed the breath of *six-fold* rings, thus reducing the D peak intensity. Meanwhile, the internal stress increased the bond energy of sp^2 atoms i.e., the wavenumber of the G peak. Stage 2 marked the onset of the chemical changes in the CNCs. Prolonged ethanol soaking increased the number of CO- and C = O bonds, which resulted in the transformation of the sp^2 state of carbon atoms into the sp^3 state or another type of sp^2 state, in which π electrons were closer to O atoms. This reduced the in-plane bond-stretching (I_G) intensity. Owing to the effect of π bonds, the C-C bond energy of sp^2 sites was larger than that of sp^3 sites. The decrease in the number of π electrons and their localization resulted in a slight decrease in the bond energy, thus reducing the wavenumber of the G peak. It should be noted that the partial transformation of sp^2 sites to other saturation sites resulted in an increase in the bandwidth of the G peak (Fig. 6c).

The physical and chemical structures of CNCs affect their physical properties. The electrical conductivity of CNCs depends on the concentration of free electrons (unlocalized π electrons) and the hopping barrier between sp^2 grains (localized states). The thermal diffusivity of CNCs depends on boundary scattering, defects scattering, and phonon frequencies. In order to investigate the effect of structural changes on

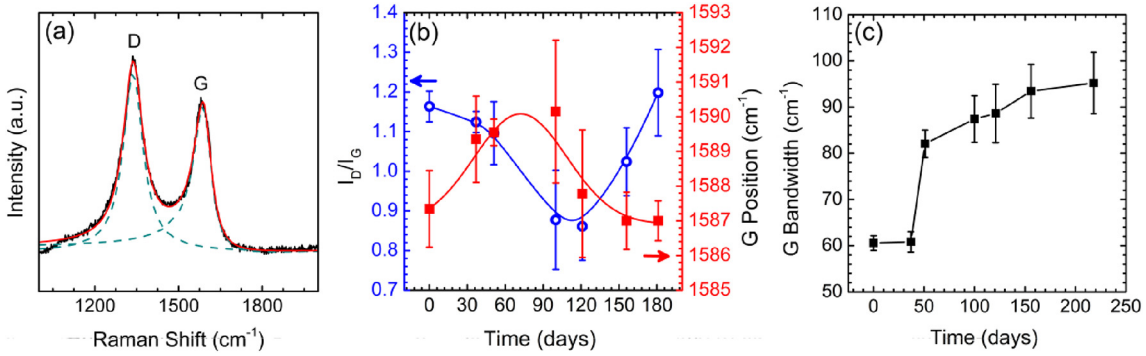

Fig. 6. Raman characterization of the CNCs. (a) Typical Raman spectrum of CNCs. (b) The intensity ratio of D to G peaks (I_D/I_G) and wavenumber of the G peak for the CNCs soaked in ethanol for different durations. (c) G peak bandwidth of the CNCs soaked in ethanol for different durations.

Table 1
Thermal diffusivities (α) and electrical conductivities (σ) of the CNCs soaked in ethanol for different durations; d is the fiber diameter of the CNCs.

Soak time (days)	Sample	d (nm)	α (10^{-7} m^2/s)	σ (10^4 S/m)
0	1	456	10.3	0.597
	2	317	21.0	1.189
	3	353	13.8	0.866
107	4	336	6.8	0.412
185	5	301	7.5	0.728
200	6	354	8.7	0.449

the physical properties of the CNCs soaked in ethanol for different durations, their thermal diffusivities and electrical conductivities were measured (Table 1).

As can be observed from Table 1, two groups of CNCs were examined. The CNCs in the first group were not soaked in ethanol. The average thermal diffusivity and electrical conductivity of the three CNC samples in this group were 15.0×10^{-7} m^2/s and 88.4 S/cm, respectively. The second group consisted of CNCs soaked ethanol for 100–200 days. These CNCs showed thermal diffusivities and electrical conductivities significantly lower than those of the first group CNCs. The average thermal diffusivity and electrical conductivity of this group were 7.7×10^{-7} m^2/s and 52.9 S/cm, respectively.

The physical changes increased the distance between the sp^2 grains, thus increasing the hopping barrier of the electrons between the localized states and the defects scattering of phonons in the amorphous sp^3 network. On the other hand, the chemical changes decreased the concentration of π electrons. The introduction of functional groups altered the phonon distribution and increased the boundary-phonon and phonon-phonon scattering significantly. The increased hopping barrier and decreased concentration of π electrons reduced the electrical conductivity of the CNCs, while the increased phonon scattering and the altered phonon distribution decreased the thermal diffusivity of the CNCs.

In order to examine the changes in the hopping barrier of the CNCs, their temperature-dependent resistance was measured. Fig. 7a shows a typical *resistance-T* curve of a single CNC. With a decrease in temperature from 290 to 150 K, the resistance increased from 232 to 274 kΩ. The resistance of CNCs can be expressed as $R = R_0 e^{E_0/kT}$, where E_0 is the hopping barrier for electrons hopping between the nearest sp^2 grains and k is the Boltzmann constant. Fig. 7b shows the linear relationship between $\mathrm{Ln}(R/R_0)$ and $1/T$ for four CNC samples. The slopes correspond to E_0/k. The hopping barriers of the CNCs were calculated from the slopes of their $\mathrm{Ln}(R/R_0)$ vs. $1/T$ curves. For comparison, the intercepts of the linear curves were adjusted to the same value. The samples with the hopping barriers of 3.13 and 3.75 meV were not soaked in ethanol, while those with the hopping barriers of 5.13 and 8.41 meV were soaked in ethanol for 228 days. Unlike the annealing-induced improvement in the graphitization of CNCs, the improvement in their sp^2 arrangement through ethanol soaking is a result of the intention for reducing the inner stress brought by ethanol, which is passive. An increase in the internal stress results in the separation of sp^2 grains and the graphite layers present in them. CNCs transform from a close-packed structure to a relatively loose structure. The permeation of ethanol improves the order degree of sp^2 grains and increases the distance between them. One may have a query, that is, whether this physical change and ethanol permeation are invertible if we pump ethanol molecules out from CNCs in vacuum. However, our results obtained by carrying out experiments in vacuum (< 1 Pa) for up to 10 h negate this hypothesis. During these experiments, the resistance of the CNCs remained quite stable. Unlike the intense chemical reactions triggered by acid or plasma treatments, the chemical changes induced by ethanol are quite slow, and hence induce physical changes. In this study, ethanol acted as a very weak oxidant. We believe that water (H_2O), which is another common solvent, will exhibit similar effects on the properties of CNCs. However, further investigation is required to confirm this.

Ethanol soaking not only changes the electrical and thermal properties of the CNCs but also altered other physical properties. Owing to their helical morphology, the mechanical properties of CNCs are affected by the sliding of graphite layers and sp^2 grains. While the arrangement of sp^2 grains improves and inner stress arises, the elastic constant of CNCs would decrease. The introduction of functional groups and the changes in the physical structure of CNCs affect their electronic properties as well. Ma et al. recorded the photoluminescence spectrum of CNCs and observed four emission peaks [36]. Since CNCs possess a polycrystalline-amorphous structure, the localization of electrons induced by sp^2 nano-grains and amorphous sp^3 networks plays an important role in altering their electronic structure. Ethanol soaking may significantly affect the PL properties of CNCs.

4. Conclusion

The effects of ethanol (a common solvent) soaking on the structure and physical properties of polycrystalline-amorphous CNCs were investigated. The CNCs were soaked in ethanol for up to one year. Ethanol molecules permeated into the CNCs through defects and vacancies. Initially, the permeation of ethanol generated an internal stress in the CNCs, which resulted in the rearrangement of sp^2 grains to reduce the internal stress. Ethanol molecules increased the distance between the sp^2 grains and that between the graphite layers within the sp^2 grains. However, the homogeneity of the (002) plane interlayer spacing also improved. With an increase in the soak time, chemical reactions started occurring slowly in the CNCs. The CO– and C=O bond contents increased, which facilitated the transformation of the sp^2 sites to other saturation sites. This transformation reduced the intensity of the G peak and its wavenumber, concentration of π electrons, and altered

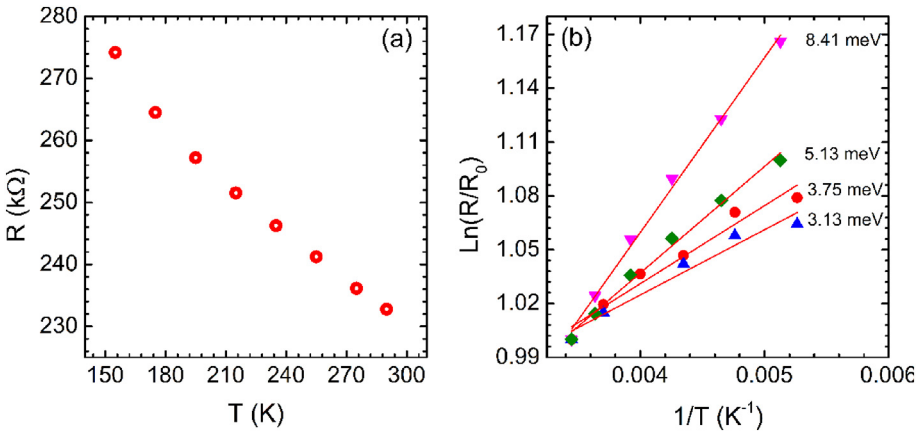

Fig. 7. (a) Temperature-dependent resistance (R) of a single CNC sample. (b) Linear relationship between Ln(R) and 1/T for four CNC samples, where the hopping barriers of 3.13 and 3.75 meV correspond to the samples not soaked in ethanol, while the hopping barriers of 5.13 and 8.41 meV correspond to the samples soaked in ethanol for 228 days.

distribution and boundary scattering of phonons as well. These physical and chemical changes reduced the electrical conductivity and thermal diffusivity of the CNCs significantly and increased the hopping barrier.

Acknowledgements

This work was supported by the National Natural Science Foundation of China (No. 51661145025, 11274055, 61520106013).

References

[1] S. Iijima, Helical microtubules of graphitic carbon, Nature 354 (6348) (1991) 56–58.
[2] S. Ihara, S. Itoh, K. Ji, Toroidal forms of graphitic carbon, Phys. Rev. B Condens. Matter 47 (19) (1993) 12908.
[3] S. Amelinckx, X.B. Zhang, D. Bernaerts, X.F. Zhang, V. Ivanov, J.B. Nagy, A formation mechanism for catalytically grown helix-shaped graphite nanotubes, Science 265 (5172) (1994) 635.
[4] M. Sevilla, A.B. Fuertes, Easy synthesis of graphitic carbon nanocoils from saccharides, Mater. Chem. Phys. 113 (1) (2009) 208–214.
[5] A. Volodin, C.V. Haesendonck, R. Tarkiainen, M. Ahlskog, A. Fonseca, J.B. Nagy, AFM detection of the mechanical resonances of coiled carbon nanotubes, Appl. Phys. A Mater. Sci. Process. 72 (1) (2001) (S75-S8).
[6] N. Tang, W. Kuo, C. Jeng, L. Wang, K. Lin, Y. Du, Coil-in-coil carbon nanocoils: 11 gram-scale synthesis, single nanocoil electrical properties, and electrical contact improvement, ACS Nano 4 (2) (2010) 781.
[7] C. Li, L. Pan, C. Deng, P. Wang, Y. Huang, H. Nasir, A flexible, ultra-sensitive strain sensor based on carbon nanocoil network fabricated by an electrophoretic method, Nanoscale 9 (28) (2017) 9872.
[8] C. Deng, L. Pan, D. Zhang, C. Li, H. Nasir, A super stretchable and sensitive strain sensor based on a carbon nanocoil network fabricated by a simple peeling-off approach, Nanoscale 8 (2017) 16404–16411.
[9] Alexander Volodin, Dieter Buntinx, Markus Ahlskog, Antonio Fonseca, J.B. N, C.V. Haesendonck, Coiled carbon nanotubes as self-sensing mechanical resonators, Nano Lett. 4 (9) (2004) 1775–1779.
[10] C. Li, L. Pan, C. Deng, P. Wang, CNC-Al_2O_3-Ti: a new unit for micro scale strain sensing, RSC Adv. 6 (109) (2016).
[11] H. Ma, L. Pan, Q. Zhao, W. Peng, Near-infrared response of a single carbon nanocoil, Nanoscale 5 (3) (2013) 1153.
[12] C.C. Su, C.L. Huang, S.H. Chang, Fabrication of aligned carbon nanocoil thermal sensor with a high temperature coefficient of electrical resistance at 25–100 °C, IEEE Trans. Nanotechnol. 14 (5) (2015) 794–797.
[13] L. Pan, Y. Konishi, H. Tanaka, O. Suekane, T. Nosaka, Y. Nakayama, Effect of morphology on field emission properties of carbon nanocoils and carbon nanotubes, Jpn. J. Appl. Phys. 44 (4A) (2005) 1652–1654.
[14] K.J. Chung, N.W. Pu, M.J. Youh, Y.M. Liu, M.D. Ger, K. Cheng, et al., Improvement of field-emission-lamp characteristics using nitrogen-doped carbon nanocoils, Diam. Relat. Mater. 53 (2) (2015) 1–10.
[15] J. Zhao, J. Wu, J.W. Jiang, L. Lu, Z. Zhang, T. Rabczuk, Thermal conductivity of carbon nanocoils, Appl. Phys. Lett. 103 (23) (2013) 635.
[16] R. Cui, L. Pan, D. Zhang, H. Nasir, Electromagnetic microwave absorption properties of carbon nanocoils/tissue, Diam. Relat. Mater. 77 (2017) 53–56.
[17] M. Sevilla, G. Lota, A.B. Fuertes, Saccharide-based graphitic carbon nanocoils as supports for PtRu nanoparticles for methanol electrooxidation, J. Power Sources 171 (2) (2007) 546–551.
[18] R.I. Jafri, N. Rajalakshmi, S. Ramaprabhu, Nitrogen-doped multi-walled carbon nanocoils as catalyst support for oxygen reduction reaction in proton exchange membrane fuel cell, J. Power Sources 195 (24) (2010) 8080–8083.
[19] T. Gohara, K. Takei, T. Arie, S. Akita, Reduction of carbon byproducts for high-purity carbon nanocoil growth by suppressing catalyst collision, Carbon 89 (2015) 225–231.
[20] J. Sun, A.A. Koós, F. Dillon, K. Jurkschat, M.R. Castell, N. Grobert, Synthesis of carbon nanocoil forests on $BaSrTiO_3$ substrates with the aid of a Sn catalyst, Carbon 60 (12) (2013) 5–15.
[21] W.Y. Sung, J. Girl Ok, W.J. Kim, S.M. Lee, S.C. Yeon, H.Y. Lee, et al., Synthesis and field emission characteristics of carbon nanocoils with a high aspect ratio supported by copper micro-tips, Nanotechnology 18 (18) (2007) 245603.
[22] V. Celorrio, L. Calvillo, S. Pérez-Rodríguez, M.J. Lázaro, R. Moliner, Modification of the properties of carbon nanocoils by different treatments in liquid phase, Microporous Mesoporous Mater. 142 (1) (2011) 55–61.
[23] H. Ma, K. Nakata, L. Pan, K. Hirahara, Y. Nakayama, Relationship between the structure of carbon nanocoils and their electrical property, Carbon 73 (1) (2014) 71–77.
[24] K. Hirahara, K. Nakata, Y. Nakayama, Non-linear annealing effect on correlation between crystallinity and oscillation of carbon nanocoils, Mater. Sci. Eng. A 595 (5) (2014) 205–212.
[25] Knez M. Tuning of optical properties by atomic layer deposition. Advanced Fabrication Technologies for Micro/Nano Optics and Photonics VI; p. 86130B-B-7.
[26] C. Deng, L. Pan, C. Li, X. Fu, R. Cui, H. Nasir, Helical gold nanotube film as stretchable micro/nanoscale strain sensor, J. Mater. Sci. (2017) 1–12.
[27] D. Li, L. Pan, S. Wu, S. Li, An active surface enhanced Raman scattering substrate using carbon nanocoils, J. Mater. Res. 28 (16) (2013) 2113–2123.
[28] W.H. Choi, M.J. Choi, J.H. Bang, Nitrogen-doped carbon nanocoil array integrated on carbon nanofiber paper for supercapacitor electrodes, ACS Appl. Mater. Interfaces 7 (34) (2015) 19370.
[29] M. Yokota, Y. Hosokawa, Y. Shinohara, T. Kawabata, K. Takimoto, Y. Suda, et al., Splitting and flattening of helical carbon nanofibers by acid treatment, J. Nanosci. Nanotechnol. 10 (6) (2010) 3910.
[30] D.W. Li, L.J. Pan, J.J. Qian, H. Ma, High efficient synthesis of carbon nanocoils by catalysts produced by a Fe and Sn containing solution, Adv. Mater. Res.-Switz 60-61 (2009) 251–255.
[31] J. Guo, X. Wang, T. Wang, Thermal characterization of microscale conductive and nonconductive wires using transient electrothermal technique, J. Appl. Phys. 101 (6) (2007) (2996-125).
[32] C. Deng, Y. Sun, L. Pan, T. Wang, Y. Xie, J. Liu, et al., Thermal diffusivity of single carbon nanocoil: uncovering the correlation with temperature and domain size, ACS Nano 10 (10) (2016).
[33] X. Chen, S. Zhang, D.A. Dikin, A. Weiqiang Ding, R.S. Ruoff, L.P. And, et al., Mechanics of a carbon nanocoil, Nano Lett. 3 (9) (2003) 1299–1304.
[34] J.A. Yan, L. Xian, M.Y. Chou, Structural and electronic properties of oxidized graphene, Phys. Rev. Lett. 103 (8) (2009) 086802.
[35] A.C. Ferrari, J. Robertson, Interpretation of Raman spectra of disordered and amorphous carbon, Phys. Rev. B Condens. Matter 61 (20) (2000) 14095–14107.
[36] H. Ma, L. Pan, Q. Zhao, Z. Zhao, J. Zhao, J. Qiu, Electrically driven light emission from a single suspended carbon nanocoil, Carbon 50 (15) (2012) 5537–5542.